JOURNAL OF AGRICULTURAL AND FOOD CHEMISTRY

Analysis of Two Bentonites of Enological Interest before and after Commercial Activation by Solid Na_2CO_3

RÉGIS D. GOUGEON,† MICHEL SOULARD,§ JOCELYNE MIEHÉ-BRENDLÉ,§ JEAN-MICHEL CHÉZEAU,§ RONAN LE DRED,§ PHILIPPE JEANDET,*,† AND RICHARD MARCHAL†

Laboratoire d'Oenologie, URVVC UPRES EA 2069, Université de Reims, Faculté des Sciences, Moulin de la Housse, B.P. 1039, 51687 Reims Cedex 2, France, and Laboratoire de Matériaux Minéraux, Université de Haute Alsace, UPRES-A-CNRS 7016, 3 Rue A. Werner, 68093 Mulhouse Cedex, France

Two natural calcium-rich bentonites used for the removal of wine proteins, originating from Greece and Turkey, were studied by X-ray diffraction, thermal analysis, and solid state NMR, before and after activation by solid Na_2CO_3. Exchange of Ca^{2+} by Na^+ mainly occurs for cations located at the edge of layers and only weakly for interlayer cations. This Na_2CO_3 activation process leads to an increased efficiency in the adsorption process of bovine serum albumin (BSA) used as a model protein for both bentonites. A direct correlation is observed between the extent of Ca^{2+}/Na^+ exchange, the strength of adsorption of BSA, and the extent of unfolding of BSA backbone.

KEYWORDS: Bentonite; Na_2CO_3 activation; bovine serum albumin; X-ray diffraction; differential thermal analysis; thermogravimetry; NMR

INTRODUCTION

One of the most common instabilities in white and rosé wines is the appearance of protein hazes in the bottle. This is the result of several factors such as pH, ionic strength, ethanol concentration, temperature, or composition of the wine, which all influence the interaction of proteins with the wine medium (*1*−*4*). However, little is known of the extent to which these factors influence the precipitation of proteins, although there are many data available concerning wine proteins (*5*−*7*). To overcome this problem during the elaboration of wines, different approaches have been considered, which basically rely on the removal of proteins. To that purpose, the bentonite treatment, which has been used for more than 60 years (*8*), is still given particular attention currently (*1*, *9*). It must be noted that since 1960, this treatment is also used for musts and, in the case of Champagne, to improve yeast elimination as a riddling adjuvant (*10*).

Bentonite is the commercial designation of a natural clay mineral, the main component of which is montmorillonite, a 2:1 dioctahedral smectite. Montmorillonite possesses a two-dimensional crystalline structure based on staked layers of tetrahedra, octahedrs, and tetrahedra connected to each other by oxygen bridges (**Scheme 1**). Whereas tetrahedra are made of silicon, octahedra are mainly made of aluminum and magnesium, which is described as octahedral substitution (of Mg for Al). This substitution provides a net negative charge to the montmorillonite, which is distributed over the complete oxygen framework and which is balanced by exchangeable cations. These cations, mainly Na^+ and Ca^{2+}, are localized within the interlayer space, and their ratio can vary significantly from one deposit to another. The particular affinity of proteins for bentonites is based on the commonly high specific surface areas associated with swelling and cation-exchange properties of the latter. Proteins of wines with an isoelectric point (Ip) value above the pH of wine (3−3.5) are positively charged, and their adsorption on bentonite is basically described as a cation-exchange process (*11*), based on electrostatic, hydropho-

Scheme 1. Representation of the Two-Dimensional Crystalline Structure of Montmorillonite

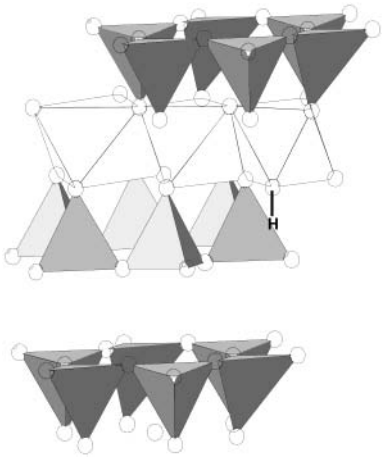

* Corresponding author (fax +33 3 26 91 33 40; e-mail philippe.jeandet@univ-reims.fr).
† Université de Reims.
§ Université de Haute Alsace.

10.1021/jf0212237 CCC: $25.00 © 2003 American Chemical Society
Published on Web 06/06/2003

Table 1. Elemental Analysis (Weight Percent) of Si, Al, Fe, Na, and Ca, As Determined by Flame Absorption Spectroscopy, and Weight Loss at 900 °C (H_2O), As Determined by TG Analysis

bentonite	SiO_2	Al_2O_3	Fe_2O_3	Na_2O	CaO	H_2O
G	46.6	26.7	3.2	0.9	2.0	19.3
GA	46.2	25.4	3.0	4.6	1.9	19.5
T	53.3	27.0	0.7	1.6	1.7	17.7
TA	51.3	25.4	0.7	4.3	1.7	19.6

bic, and/or hydrophilic interactions (*12*, *13*). Proteins with no overall positive charge or negative charge can also be adsorbed by other mechanisms such as hydrogen-bonding mechanism or van der Waals interactions (*14*). It is considered that a Na^+-rich bentonite (high Na^+/Ca^{2+} ratio) is more efficient for protein removal than bentonites having a higher content of other interlayer cations such as calcium (*11*). However, many natural deposits contain calcium-rich bentonites, and, therefore, to be more efficient these natural bentonites undergo a commercial activation process that consists of a solid treatment of the wet mud by solid Na_2CO_3 (~3% w/w), at a temperature of 80 °C. The aim of this activation is to obtain a sodium-rich bentonite as a result of the Na−Ca cation exchange, according to the equation

$$\text{montmorillonite}-Ca^{2+} + Na_2CO_3 \rightarrow \text{montmorillonite}-2Na^+ + CaCO_3$$

Although the effect of this activation is known (*15*, *16*), fine modifications undergone by the bentonites and their correlation to the protein adsorption efficiency remain ignored. Therefore, this paper reports a multiple-technique analysis of two natural enological bentonites, which were selected before and after Na_2CO_3 activation. They were studied by powder X-ray diffraction, thermogravimetry (TG)−differential thermal analysis (DTA), and multinuclear solid state NMR. Bovine serum albumin (BSA) was chosen as a protein representative and adsorbed on both samples before and after activation in order to correlate the amount of adsorbed species to the Na_2CO_3 activation process.

MATERIALS AND METHODS

Samples. A bentonite from the Greek island of Milos and another one from Turkey were selected before and after Na_2CO_3 activation and supplied by the Société Française de Bentonites et Dérivés (Tréport, France). The four as-received samples consisted of wet coarsely ground powders. After drying at 50 °C for 2 days, samples were finely ground and kept either under controlled humidity ($P/P_0 = 0.79$) or in ambient atmosphere ($P/P_0 \sim 0.55$). Throughout the text, these four samples will be labeled G and GA for the Greek bentonite before and after activation, respectively, and T and TA for the Turkish bentonite before and after activation, respectively. The elemental analysis (Na, Ca, Si, Al, Fe) of the samples, obtained by flame absorption spectroscopy, is given in **Table 1**.

BSA, which is a large water-soluble protein (MW = 66000, Ip ~ 4.4), was purchased from Fluka, Riedel-de Haën (Hanover, Germany), and used as received. For the adsorption, 1.2 g of each of the four bentonites was first mixed, for 12 h, with 25 mL of a model wine solution composed of, for a volume of 100 mL, deonized water, 12 mL of ethanol, 300 mg of tartaric acid, 400 mg of glycerol, and 10 mg of NaCl and buffered to a pH of 3.3 using KOH. Each of these four suspensions was subsequently mixed with a separate solution of 120 mg of BSA in 50 mL of model wine, for 6 h under stirring and then for 24 h without stirring. After filtration and/or centrifugation and repeated washes with the model wine and deionized water, the four BSA-adsorbed samples, G−BSA, GA−BSA, T−BSA, and TA−BSA, were dried overnight at room temperature in air and kept under controlled humidity ($P/P_0 = 0.79$).

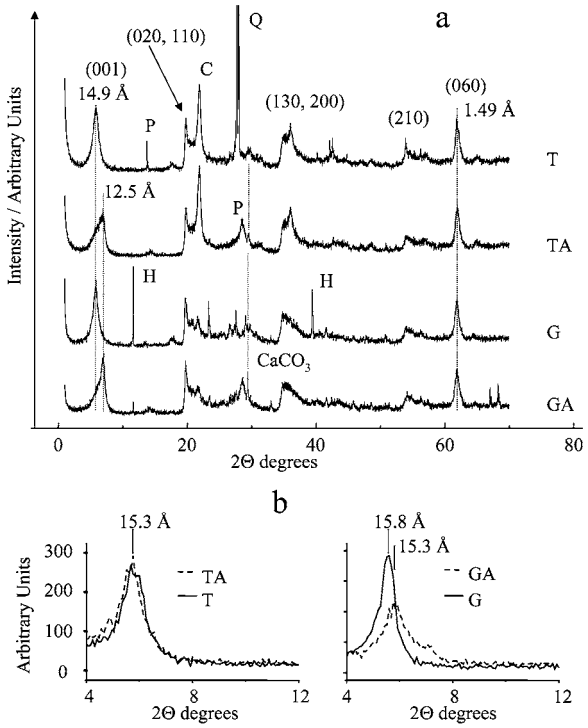

Figure 1. (a) Powder X-ray diffraction patterns recorded under ambient humidity conditions ($P/P_0 \sim 0.55$). Characteristic bands of montmorillonite are indicated by their *hkl* reflections, and peaks of nonclay minerals are identified by the following letters: Q, quartz; C, cristoballite; P, plagioclase; H, hydrotalcite. Dashed gray lines highlight the two d_{001} distances, the $CaCO_3$ characteristic peak and the d_{060} distance. (b) (001) reflections recorded under controlled humidity ($P/P_0 = 0.79$).

X-ray Powder Diffraction. X-ray powder diffractograms were recorded either with a STOE STADI-P powder X-ray diffractometer (Darmstadt, Germany), equipped with a linear position-sensitive detector (6° 2Θ) in Debye−Scherrer geometry and employing the Ge monochromated Cu $K_{\alpha 1}$ radiation ($l = 1.5406$ Å), or with a Philips PW-1800 powder X-ray diffractometer (Amsterdam, The Netherlands). The former permitted a controlled atmosphere with capillaries, which were filled with powder kept under controlled humidity, just before the start of the experiment.

Thermal Analysis. TGA-DTA measurements were carried out on a Setaram Labsys apparatus (Caluire, France) under air flow conditions, with a heating rate of 5 °C min^{-1}, between 20 and 800 or 900 °C.

Solid State NMR. ^{23}Na and ^{13}C NMR experiments were run on a Bruker DSX 400 spectrometer (Wissembourg, France) operating at frequencies of 105.8 and 100.6 MHz, respectively. ^{23}Na MAS spectra were acquired with a standard Bruker double-channel 4-mm probe, at a spinning frequency of 10 kHz, whereas $^1H-^{13}C$ cross-polarization magic angle spinning (CP-MAS) spectra were acquired with a Bruker double-channel 7-mm probe, at a spinning frequency of 4 kHz. Hartmann−Hahn matching for the $^1H-^{13}C$ CP-MAS experiments was set on adamantane with ^1H and ^{13}C radio frequency fields of ~60 kHz. Chemical shifts for ^{23}Na and ^{13}C spectra were referenced to 1 M NaCl solution and adamantane, respectively. Deconvolution of the spectra was realized with the WINFIT software (*17*).

RESULTS

Characterization of the Bentonites. *Powder X-ray Diffraction.* **Figure 1a** shows the powder X-ray diffractograms of the four samples, recorded under ambient humidity conditions ($P/P_0 \sim 0.55$), and **Figure 1b** magnifies the four d_{001} regions, recorded under controlled humidity ($P/P_0 = 0.79$). Each diffractogram exhibits *hkl* bands at 4.45−4.48 Å (020, 110), 2.52−2.58 Å (130, 200), and 1.67−1.70 Å (210), which are

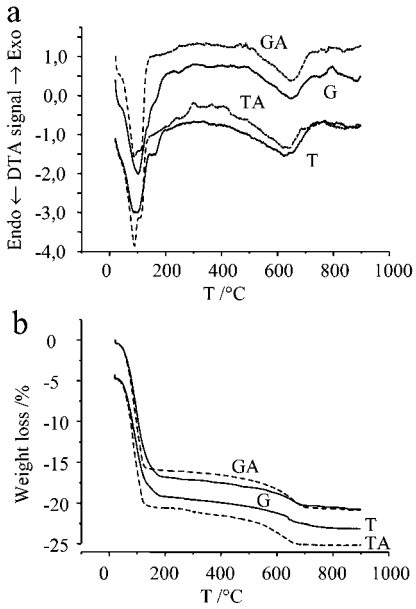

Figure 2. Differential thermal analysis (a) and thermogravimetry (b) curves of the four bentonites.

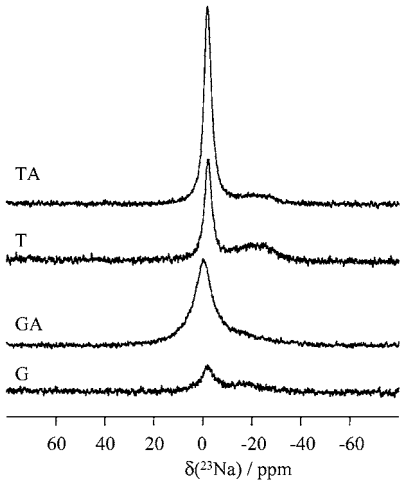

Figure 3. ^{23}Na magic angle spinning nuclear magnetic resonance spectra of the four bentonites, recorded with a pulse duration of 2 μs (π/6), a recycle delay of 1 s, and 2000 transients.

Table 2. Relative Intensity (Percent) of the Two ^{23}Na MAS NMR Peaks of the Four Bentonites

bentonite	high-frequency peak	low-frequency peak
G	61	39
GA	89	11
T	64	36
TA	87	13

characteristic of a montmorillonite (*18*). The unique signal at 1.49 Å (060) clearly indicates the similar dioctahedral nature of the two bentonites, that is, with vacancies in the octahedral sheet. The position of the (001) peak is a direct indication of the basal spacing (d_{001}), which is equal to the sum of the interlayer spacing and the thickness of the layer (~9.6 Å for a 2:1 phyllosilicate). Under ambient atmosphere conditions, the two unactivated samples exhibit a (001) band at 14.9 Å. After activation, the maximum is shifted to a lower value of 12.5 Å, but a shoulder centered at 14.9 Å is still observed for both GA and TA, indicating that interlayer Ca^{2+} ions are still present (*19*). However, the intensity ratio between the 12.5 Å peak and the 14.9 Å shoulder is higher for GA than for TA, and the characteristic narrow peak for $CaCO_3$ is more clearly observed for GA than for TA, suggesting a better Na^+/Ca^{2+} exchange for the Greek bentonite. When recorded under controlled humidity ($P/P_0 = 0.79$), the (001) peaks do not vary so significantly from the unactivated to the activated samples (**Figure 1b**). For the Turkish bentonite, the d_{001} distance of 15.3 Å is the same before and after activation, whereas for the Greek bentonite, it slightly decreases from 15.8 to 15.3 Å upon activation. Under this controlled humidity, high values of 15.3−15.8 Å are typical of montmorillonite with a high content of Ca^{2+} ions in its interlayer spaces (*19*). Before activation, the higher d_{001} distance of G compared to that of T is in agreement with the higher Ca^{2+}/Na^+ ratio of the former (**Table 1**). However, these results are consistent with those obtained under ambient humidity conditions; that is, the Na^+/Ca^{2+} exchange has been more efficient in GA than in TA.

Figure 1a indicates that montmorillonite is the major component of the four samples. However, minor amounts of quartz, cristoballite, and plagioclase ($NaAlSi_3O_8$ or $CaAl_2Si_2O_8$) are also identified in the four samples, with, in addition, some hydrotalcite-type minerals for the Greek bentonite. Repeated acquisitions for a given sample showed that although the intensity of some of the peaks could vary significantly from one pattern to the other (for instance, quartz in the Turkish bentonite), the amount of nonclay inorganic minerals remained unchanged upon activation. This observation was further confirmed by ^{29}Si and ^{27}Al solid state NMR spectra (data not shown).

Thermal Analyses. Each sample exhibits a major endotherm at 100 °C (**Figure 2a**), which corresponds to montmorillonite dehydration. A second strong endotherm is observed for all of the samples at ~650 °C, which is related to dehydroxylation of the montmorillonite (*20*). Weak exothermic signals may also be considered for TA between 250 and 450 °C, which are probably due to organic impurities. The corresponding curves of weight loss (**Figure 2b**) consistently show a major step for dehydration followed by the second weight loss at higher temperatures, for dehydroxylation. As expected due to the addition of Na_2CO_3, the overall weight loss at 900 °C is higher for the activated bentonites than for the unactivated ones (**Table 1**). However, whereas a weak endotherm observed for the two activated samples at ~120 °C can possibly be attributed to $CaCO_3$ dehydration (**Figure 2a**), no distinct endothermic signal for the decomposition of calcium carbonate can be seen at ~800 °C.

Solid State NMR. ^{23}Na MAS NMR spectra of the four bentonites (**Figure 3**) are characterized by a narrow peak at ~ −1 ppm and a broader one centered at −18 and − 22 ppm for the Greek and Turkish bentonites, respectively. The corresponding relative intensities are gathered in **Table 2**. These two signals indicate two distinct environments for Na^+ cations in the bentonites, which can be explained by two levels of hydration. Highly hydrated Na^+ ions, which exhibit an almost liquidlike behavior (−2 ppm), can be found at the edge of the silicate layers, whereas interlayer Na^+ ions, which are less accessible to hydration and in more constrained environments, will give rise to a broader signal resonating at lower frequencies. Upon activation, the main difference is an increased intensity in the high-frequency signal relative to that of the broader signal for both TA and GA (**Table 2**), which indicates that Na^+ enrichment has mainly occurred at the periphery of silicate layers.

Adsorption of BSA. *Thermal Analyses.* Upon adsorption of BSA, the DTA curve of each sample is dominated by essentially two exothermic signals between 200 and 650 °C (**Figure 4a**), which correspond to the oxidation of the adsorbed organic matter. For both the Turkish and Greek bentonites, the first

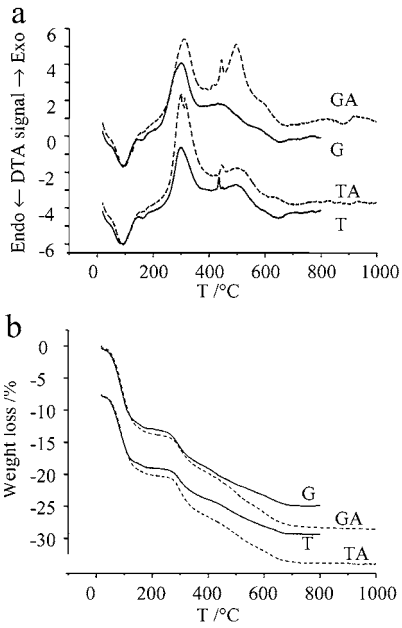

Figure 4. Differential thermal analysis (a) and thermogravimetry (b) curves of the four bovine serum albumin-adsorbed bentonites.

Table 3. Weight Percent Amounts of BSA Adsorbed on the Four Bentonites, from TG Analysis

bentonite	BSA	bentonite	BSA
G	8.7	T	6.7
GA	10.5	TA	9.5

exotherm is more intense in the activated sample than in the unactivated one. For the Turkish bentonite, the second exotherm has the same intensity before and after activation. In contrast, for the Greek bentonite, the second exotherm is significantly more intense in the activated sample than in the unactivated one, indicating a more energetic oxidation process. Endotherms for dehydration are still observed at 100 °C, but with slightly weaker intensity than before adsorption, and endotherms for dehydroxylation, at 650 °C, are now partly covered by the tail of the exothermic signals. These observations on DTA curves can be consistently related to the weight loss curves (**Figure 4b**). For each sample, the initial weight loss due to dehydration is immediately followed above 250 °C by the weight loss due to the oxidation of BSA (**Table 3**). For both the Turkish and Greek bentonites, the weight loss due to the oxidation of BSA is higher for the activated samples than for the unactivated ones, which is consistent with the positive effect of the activation on the adsorption efficiency.

Solid-State NMR. ^{13}C CP-MAS NMR spectra of G−BSA, GA−BSA, and TA−BSA are displayed in **Figure 5**, along with the spectrum of pure BSA. Different peaks can be resolved in the spectrum of BSA. However, upon adsorption on bentonites, the spectrum of BSA is characterized by a significant decrease in the signal-to-noise ratio and a loss of resolution of all signals except those of carboxylic and carbonyl groups, which prevents a detailed analysis of all the different signals. It must be noted that the higher loss of resolution observed for the spectra of G−BSA and GA−BSA can undoubtly be related to the paramagnetic effect due to the higher iron content of these two samples (**Table 1**). The C═O region in the spectrum of G−BSA resembles that of pure BSA, although with a broadening and shift to lower frequencies (**Table 4**). In contrast, for both GA−BSA and TA−BSA, two peaks, shifted to lower frequencies, are now resolved for the carboxylic and carbonyl groups. Moreover, for GA−BSA, the shift is more pronounced for the

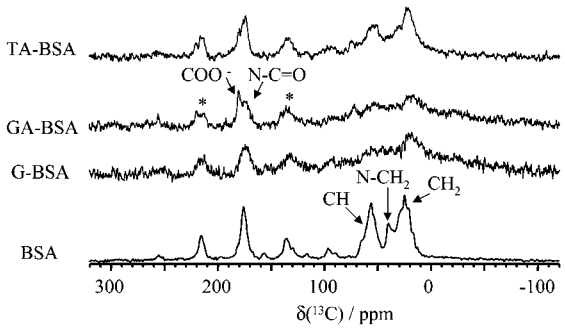

Figure 5. ^{1}H–^{13}C cross-polarization magic angle spinning nuclear magnetic resonance spectra, recorded with a recycle delay of 3 s and 1888 transients for pure bovine serum albumin (BSA) and with a recycle dealy of 2 s and 6000 transients for BSA-adsorbed bentonites. *, spinning sidebands.

Table 4. Carboxylic (COO^-) and Carbonyl (N—C═O) ^{13}C Chemical Shifts (δ) of Pure BSA and of Three BSA-Adsorbed Bentonites

sample	δ_{COO^-}	$\delta_{N-C=O}$
BSA	181	175.9
G	not observed	174.2
GA	180	173.5
TA	180	174

carbonyl group, which also slightly broadens. Such shifts to low frequencies upon adsorption of proteins on solid surfaces have been related to the adoption of more extended secondary structures (*14*, *17*).

DISCUSSION

Bentonites are universally used in wine-making for the adsorption of proteins from wines. However, whereas natural bentonites often contain calcium in their interlayer spaces, it has been shown that bentonites containing sodium can adsorb almost twice the amount of protein (*11*). Therefore, the primary purpose of the Na_2CO_3 activation of a raw bentonite is to enrich the latter in Na^+ ions.

Results of the elemental analysis clearly confirm a significant increase in the Na^+/Ca^{2+} ratio for the two bentonites. However, our measure of the variation of the basal spacing, with Na_2CO_3 activation, clearly shows that it does not systematically lead to a significant interlayer Na^+ enrichment. Indeed, for the Turkish bentonite, under controlled humidity ($P/P_0 = 0.79$), the d_{001} distance of the activated sample remains the same as that of the unactivated one. A decrease in this value is observed for the Greek bentonite only after activation, indicating that interlayer Ca^{2+} ions have been more replaced by Na^+. These observations are confirmed by ^{23}Na MAS spectra, which unambiguously show that upon activation, the significant increase in the sodium content mainly consists of the Na^+ enrichment at the edges of the interlayer spaces. It is likely, however, that a Na^+/Ca^{2+} exchange partly occurs even for the Turkish bentonite, because XRD patterns recorded under ambient conditions show a similar modification of the 001 peak for the two bentonites.

Both GA and TA adsorb higher amounts of BSA than G and T, respectively, which confirms the increased efficiency provided by Na_2CO_3 activation. However, our results clearly show that adsorption has not proceeded similarly for the Greek and Turkish bentonites. As indicated by TG-DTA analyses, adsorption already occurs before Na_2CO_3 activation, and ^{13}C NMR shows that it is accompanied by a weak unfolding of the protein backbone. It is interesting to note that such ^{13}C NMR observa-

tion of the loss of helicity of BSA adsorbed on bentonite is in perfect agreement with a recent FTIR analysis, which emphasizes the importance of electrostatic interactions between the clay surface and the protein side-chain functional groups, in the adsorption process (*21*). After activation, the Turkish bentonite, for which XRD has shown that interlayer Ca^{2+} ions have only weakly been replaced by Na^+ ions, simply adsorbs more BSA proteins, with no changes in the profile of the oxidation exotherm compared to that of the unactivated sample. In contrast, the activated Greek bentonite, which has undergone a higher interlayer Na^+/Ca^{2+} exchange, exhibits a DTA profile with a much more intense oxidation exotherm at high temperatures. Therefore, the increase in the interlayer Na^+ content in GA is accompanied by an increase in the strength of adsorption of BSA in GA−BSA. Furthermore, ^{13}C NMR spectra indicate that the higher the increase in the strength of adsorption of BSA, the lower the chemical shift of the BSA backbone carbonyl peak. Therefore, together these results indicate that the increase in the interlayer Na^+ content is accompanied by an increase in the strength of adsorption of BSA, and this is characterized by an increase in BSA unfolding. The observed broadening of the ^{13}C NMR spectrum of the two Greek samples, due to iron that can be located both in interlayer spaces and within layers, interestingly brings a further argument in favor of the protein unfolding. Indeed, the paramagnetic effect of iron is strongly dependent on internuclear distances. Therefore, and given that this broadening is particularly pronounced for the aliphatic region of the ^{13}C NMR spectra, it can be assumed that protein side chains have necessarily come near the surface of the clay as a result of a loss of helicity of BSA (*21*).

CONCLUSION

In this paper, two natural bentonites from Greece and Turkey were studied by X-ray diffraction, thermal analysis, and solid state NMR, before and after Na_2CO_3 activation. Although activated bentonites adsorb more BSA proteins than unactivated ones, our results have shown that cation exchange mainly occurs at the edges of the bentonite silicate layers.

Together, these results show that the multiple-technique analysis of enological bentonites can bring useful new insights in the mechanism of adsorption of proteins on bentonites.

ACKNOWLEDGMENT

We warmly acknowledge A.-C. Faust for elemental analyses and the Société Française de Bentonites et Dérivés for providing bentonites.

LITERATURE CITED

(1) Achaerandio, I.; Pachova, V.; Güell, C.; López, F. Protein adsorption by bentonite in a white wine model solution: Effect of protein molecular weight and ethanol concentration. *Am. J. Enol. Vitic.* **2001**, *52*, 122−126.

(2) Dawes, H.; Boyes, S.; Keene, J.; Heatherbell, D. Protein instability of wines: Influence of protein isoelectric point. *Am. J. Enol. Vitic.* **1994**, *45*, 319−326.

(3) Mesrob, B.; Gorinova, N.; Tsakov, D. Characterization of the electrical properties and molecular weights of the proteins in white wines. *Nahrung* **1983**, *27*, 727−733.

(4) Yokotsuka, K.; Yoshii, M.; Aihara, T.; Kushida, T. Turbidity formation caused by the interaction of must proteins with wine tannins. *J. Ferment. Technol.* **1983**, *61*, 413−416.

(5) Hoj, P. B.; Tattersall, D. B.; Adams, K.; Pocock, K. F.; Hayasaka, Y.; Van Heeswijck, R.; Waters, E. J. The "haze-proteins" of wine−A summary of properties, factors affecting their accumulation in grapes, and the amount of bentonite required for their removal from wine. *Am. J. Enol. Vitic.* **2001**, *51*, 147−154.

(6) Moreno-Arribas, M. V.; Puyeo, E.; Polo, M. C. Analytical methods for the characterization of proteins and peptides in wines. *Anal. Chim. Acta* **2002**, *458*, 63−75.

(7) Ferreira, R. B.; Piçarra-Periera, M. A.; Monteiro, S.; Loureiro, V. B.; Teixeira, A. R. The wine proteins. *Trends Food Sci.* **2002**, *12*, 230−239.

(8) Saywell, L. G. Clarification of wine. *Ind. Eng. Chem.* **1934**, *26*, 981−982.

(9) Weiss, K. C.; Lange, L. W.; Bisson, L. F. Small-scale fining trials: effect of method of addition on efficiency of bentonite fining. *Am. J. Enol. Vitic.* **2001**, *52*, 275−279.

(10) Vernhet, A.; Leveau, J.-Y.; Cerf, O.; Bellon-Fontaine, M.-N. Role of electrostatic interactions in *Saccharomyces cerevisiae* adhesion to the inner surface of champagne bottles. *Biofouling* **1992**, *5*, 323−334.

(11) Blade, W. H.; Boulton, R. Adsorption of protein by bentonite in a model wine solution. *Am. J. Enol. Vitic.* **1988**, *39*, 193−199.

(12) Gougeon, R. D.; Reinhlodt, M.; Delmotte, L.; Miehé-Brendlé, J.; Chézeau, J. M.; Le Dred, R.; Marchal, R.; Jeandet, P. Direct observation of polylysine side-chain interaction with smectites interlayer surfaces through $^1H-^{27}Al$ heteronuclear correlation spectroscopy. *Langmuir* **2002**, *18*, 3396−3398.

(13) Staunton, S.; Quiquampoix, H. Adsorption and conformation of bovine serum albumin on montmorillonite: Modification of the balance between hydrophobic and electrostatic interactions by protein methylation and pH variation. *J. Colloid Interface Sci.* **1994**, *166*, 89−94.

(14) Gougeon, R. D.; Soulard, M.; Reinhlodt, M.; Miehé-Brendlé, J.; Chézeau, J. M.; Le Dred, R.; Marchal, R.; Jeandet, P. Polypeptide adsorption on a synthetic montmorillonite: A combined solid-state NMR, X-ray diffraction, thermal analysis, and N_2 adsorption study. *Eur. J. Inorg. Chem.* **2003**, 1366−1372.

(15) Karatepe, N.; Ersoy-Meriçboyu, A.; Küçükbayrak, S. Activation of $Ca(OH)_2$ using different siliceous materials. *Environ. Technol.* **1999**, *20*, 377−385.

(16) Yildiz, N.; Calimli, A.; Sarikaya, Y. The characterization of Na_2CO_3 activated Kütahya bentonite. *Turk. J. Chem.* **1999**, *23*, 309−317.

(17) Kricheldorf, H. R.; Müller, D. Secondary structure of peptides. III. ^{13}C NMR Cross polarization/magic angle spinning spectroscopic characterization of solid polypeptides. *Macromolecules* **1983**, *16*, 615−623.

(18) Reinholdt, M.; Miehé-Brendlé, J.; Delmotte, L.; Tuilier, M. H.; le Dred, R.; Cortès, R.; Flank, A. M. Fluorine route synthesis of montmorillonites containing Mg or Zn and characterization by XRD, thermal Analysis, MAS NMR and EXAFS spectroscopy. *Eur. J. Inorg. Chem.* **2001**, 2831−2841.

(19) Douglas, M. C. M.; Wilson, M. J. Interlayer and intercalation complexes of clay minerals. In *Crystal Structures of Clay Minerals and their X-ray Identification*; Mineralogical Society Monograph 5; London, U.K., 1980; pp 197−224.

(20) Cuadros, J.; Delgado, A.; Cardenete, A.; Reyes, E.; Linares, J. Kaolinite/montmorillonite resembles beidellite. *Clays Clay Miner.* **1994**, *42*, 643−651.

(21) Servagent-Noinville, S.; Revault, M.; Quiquampoix, H.; Baron, M. H. Conformational changes of bovine serum albumin induced by adsorption on different clay surfaces: FTIR analysis. *J. Colloid Interface Sci.* **2000**, *221*, 273−283.

Received for review December 17, 2002. Revised manuscript received April 11, 2003. Accepted April 13, 2003. We are grateful to the Region Champagne-Ardenne for financial support through the grant to R.D.G.

JF0212237